ACS APPLIED MATERIALS & INTERFACES

www.acsami.org

Research Article

Carbazolyl-Substituted Benzoic Anhydrides as Efficient Triplet Harvesters for High-Brightness Blue Organic Light-Emitting Diodes

Myroslava Aksionova, Khrystyna Ivaniuk, Roman Lytvyn, Stepan Kutsiy, Oskar Kaszubowski, Vasyl Kinzhybalo, Asta Dabulienė, Dmytro Volyniuk, Mykola D. Obushak, Juozas Vidas Grazulevicius,* and Mykhaylo A. Potopnyk*

Cite This: https://doi.org/10.1021/acsami.6c11053

Read Online

ACCESS | Metrics & More | Article Recommendations | Supporting Information

ABSTRACT: A simple and efficient synthetic strategy for the preparation of carbazole-based C_2-symmetric anhydrides with donor−acceptor−donor (D−A−D) architecture is presented. Four benzoic anhydrides incorporating carbazole or 3,6-di-*tert*-butylcarbazole donor units, linked to the anhydride acceptor moiety through either *para*- or *ortho*-positions, are rationally designed, synthesized, and systematically investigated. Photophysical studies reveal a strong dependence of photophysical properties on the linkage topology. While *para*-linked derivatives exhibit neither delayed fluorescence nor phosphorescence, *ortho*-substituted anhydrides display small singlet−triplet energy gaps and consequently show thermally activated delayed fluorescence (TADF), as well as unexpected room-temperature phosphorescence (RTP). Therefore, compounds bearing *ortho*-linked carbazole donor moieties are successfully employed as triplet-harvesting emitters in sky-blue organic light-emitting diodes (OLEDs), delivering electroluminescence maxima at 475 and 481 nm, maximum external quantum efficiencies of up to 21.0%, high luminance exceeding 62 000 cd/m^2, and low efficiency roll-off. These results demonstrate that the formation of anhydrides from donor-substituted aromatic acids represents a versatile and effective design strategy for highly emissive TADF/RTP materials and provides a promising platform for the development of efficient multicolor OLED emitters through rational molecular engineering.

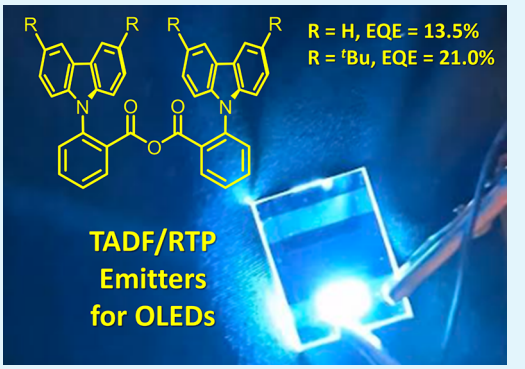

KEYWORDS: *thermally activated delayed fluorescence, room-temperature phosphorescence, electroluminescence, OLED, low efficiency roll-off*

INTRODUCTION

Over the past decades, purely organic emitters exhibiting thermally activated delayed fluorescence (TADF) and room-temperature phosphorescence (RTP) have emerged as transformative alternatives to conventional fluorescent materials and noble-metal-based phosphorescent complexes for organic light-emitting diodes (OLEDs).[1−3] The development of highly efficient blue organic light-emitting diodes (OLEDs) remains one of the major challenges in the field of organic electronics, largely due to the strict requirements for deep blue light emission and long operational life.[4−6] By enabling efficient utilization of triplet excitons, both TADF and RTP can, in principle, deliver 100% internal quantum efficiency (IQE), making them central to the development of next-generation OLED technologies.[7] Although TADF and RTP rely on distinct photophysical mechanisms, their simultaneous presence within a single molecular system has recently attracted growing interest, with several dual-emissive organic compounds reported in the literature.[8−10]

Importantly, the coexistence of TADF and RTP is not merely a photophysical curiosity but represents a compelling strategy to overcome long-standing limitations in OLED performance.[11] In purely TADF-based devices, severe efficiency roll-off at high current densities remains a critical bottleneck, commonly attributed to triplet−triplet and triplet−polaron annihilation processes.[12] In contrast, RTP-based OLEDs typically display significantly reduced roll-off and maintain higher efficiencies under high-current operation.[13−15] The integration of RTP and TADF within a single emitter therefore offers a unique opportunity for synergistic triplet harvesting, where multiple radiative decay pathways operate in parallel.[16] Such synergy has the potential to suppress efficiency roll-off, enhance operational stability, and enable robust device performance under technologically relevant

Received: June 1, 2026
Revised: August 6, 2026
Accepted: August 11, 2026

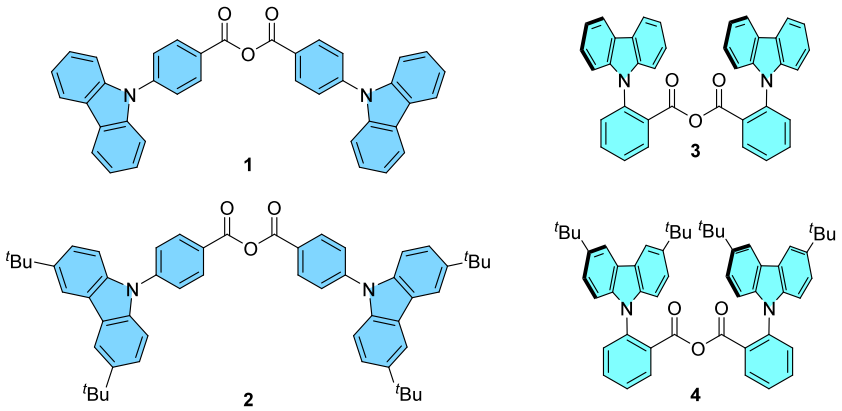

Figure 1. Anhydrides of 2- and 4-(9*H*-carbazol-9-yl)benzoic acids (**1**–**4**).

driving conditions – an outcome that remains highly challenging to achieve using conventional molecular designs.

From a molecular engineering perspective, donor–acceptor (D–A) architectures dominate the design of organic TADF and RTP materials, owing to their tunable excited-state energetics and charge-transfer character.[17] Carbazole derivatives, in particular, are among the most extensively employed donor units in the design of materials for organic optoelectronics.[4,6,18–23] While most RTP and TADF emitters are based on simple D–A motifs, donor–acceptor–donor (D–A–D) architectures have proven to be especially effective in enhancing radiative efficiency and device stability.[24] In such systems, a central acceptor unit is symmetrically flanked by two donor moieties, typically resulting in stronger charge-transfer interactions, smaller singlet–triplet energy gaps, and improved emissive performance compared to that of analogous D–A structures.[25]

Despite intense research activity in this field, the majority of reported TADF and RTP materials rely on synthetically complex acceptor units and multistep synthetic routes, which significantly increase cost and limit scalability. On the other hand, carbazolyl-substituted benzoic acids are inexpensive, readily accessible, and widely used as intermediates in synthesis of luminescent compounds and functional materials.[26–33] However, these acids have been largely overlooked as functional emitters since they do not exhibit intrinsic TADF or RTP, possess low molecular weights, show high tendencies to crystallize, and contain labile hydrogen atoms. These features are detrimental to the morphological stability of solid amorphous thin films and device stability. Overcoming these limitations in a simple and general manner remains an unmet challenge.

On the other hand, the spatial orientation of the donor and acceptor units plays an essential role in modulating the properties of TADF/RTP emitters.[34,35] In this context, *ortho*-phenylene-linked D–A compounds introduce significant steric hindrance, effectively decoupling the highest occupied molecular orbital (HOMO) and the lowest unoccupied molecular orbital (LUMO).[36–38] This spatial separation minimizes the singlet-triplet energy gap (ΔE_{ST}), thereby facilitating efficient intersystem crossing (ISC) and reverse intersystem crossing (RISC), which are essential for efficient triplet harvesting in electroluminescent devices.[39,40]

Herein, we report a straightforward approach involving the direct transformation of carbazolyl-substituted benzoic acids into corresponding anhydrides **1**–**4** (Figure 1), which leads to changes in their photophysical properties. This strategy was inspired by the serendipitous isolation of an anhydride byproduct formed during acylation reactions of 2-(9*H*-carbazol-9-yl)benzoic acid. Comprehensive nuclear magnetic resonance spectroscopy (NMR) and single-crystal X-ray diffraction (SCXRD) analyses revealed that this compound is the anhydride of 2-(9*H*-carbazol-9-yl)benzoic acid, a structure that had not previously been explored as a functional emitter.

Remarkably, despite the generally accepted high reactivity of benzoic anhydrides, the carbazolyl-substituted anhydrides exhibit exceptional chemical stability and can be recrystallized from protic solvents without decomposition. SCXRD analysis indicates that steric shielding of the carbonyl groups, combined with conjugative donation from the carbazole unit, significantly reduces electrophilicity of the anhydride moiety. This intrinsic stabilization transforms a traditionally reactive functional group into a robust acceptor core whose derivatives are suitable for optoelectronic applications.

Crucially, this simple "dimerization" approach simultaneously addresses multiple long-standing challenges in organic emitter design. Conversion of benzoic acids into anhydrides (i) results in nearly doubled the molecular weight, (ii) elimination of labile hydrogen atoms, (iii) enhancement of morphological stability of thin films, (iv) generation of an inherent D–A–D architecture without the need for complex synthetic modifications, and (v) strengthening of the acceptor unit, which is expected to reduce the ΔE_{ST}.

RESULTS AND DISCUSSION

Synthesis and Characterization

The synthesis of the target anhydrides is presented in Scheme 1. Carbazole (**5**) and 3,6-di-*tert*-butylcarbazole (**6**) were selected as starting building blocks owing to their low cost and commercial availability. In the first step, 2- and 4-(9*H*-carbazol-9-yl)benzoic acid esters (**9**–**12**) were synthesized in 66–95% yields via Ullmann coupling between carbazoles **5** and **6** and the corresponding 2- or 4-iodobenzoic acid esters (**7** and **8**).[41,42] Subsequently, esters **9**–**12** were quantitatively converted into the corresponding 2- and 4-(9*H*-carbazol-9-yl)benzoic acids (**13**–**16**) by alkaline hydrolysis upon refluxing with Potassium hydroxide in tetrahydrofuran/ethanol/water mixture following further acidification. Desired anhydrides **1**–**4** were obtained in 35–64% yields by refluxing acids **13**–**16** in acetic anhydride for 6 h. The products

https://doi.org/10.1021/acsami.6c11053
ACS Appl. Mater. Interfaces XXXX, XXX, XXX–XXX

Scheme 1. Synthesis of Anhydrides 1−4

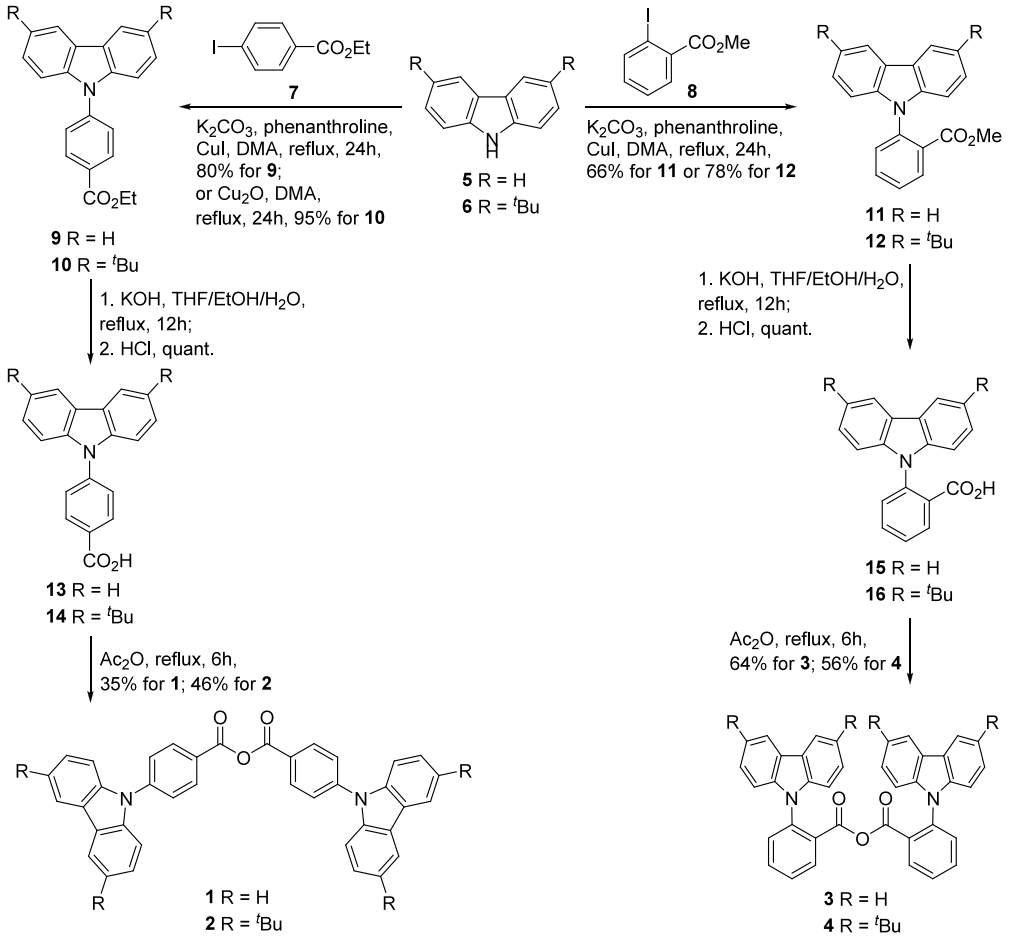

were purified by column chromatography using hexanes/dichloromethane (1:1, v/v) as the eluent. All synthesized anhydrides were fully characterized by ^{1}H and ^{13}C NMR and infrared (IR) spectroscopies, as well as by high-resolution mass spectrometry (HRMS). Additionally, the structures of compounds **1**, **3**, and **4** were confirmed by SCXRD analysis (Figures S1−S3 and Tables S1−S3 in the Supporting Information).

Compounds **1** and **4** crystallize in the monoclinic crystal system (*I*2/*a* space group), while anhydride **3** crystallizes in the triclinic crystal system (non-centrosymmetric *P*1 space group).

The asymmetric part of the unit cell of compound **1** contains half of a molecule, two-fold axis goes through the bridging O atom (Figure S4 in the Supporting Information). The dominant type of intermolecular interaction is T-stacking (i.e., C−H···π interactions; Figure S5 in the Supporting Information). There are also rather weak C−H···O hydrogen bonds in the crystal (Figure S6 in the Supporting Information). Geometric parameters of intermolecular interactions are presented in Table S4 in the Supporting Information.

Due to the two independent molecules in the asymmetric part of the unit cell that are "pseudo-enantiomers" of each other (Figure S7 in the Supporting Information), crystals of compound **3** can be treated as a kryptoracemic. This means that molecule A has an almost identical conformation to the inverted molecule B (Figure S8 in the Supporting Information). In general, kryptoracemic crystals are very rare, accounting for only about 0.2% of the crystals deposited in the Cambridge Structural Database (CSD).[43] Despite the differences in the molecular structures of compounds **1** and **3**, intermolecular interactions in crystal **3** are dominated by C−H···π contacts, as they are in crystal **1**. There are also hydrogen bonds involving oxygen atoms (Figure S9 and Table S5 in the Supporting Information).

The obtained crystals of dye **3** belong to the non-centrosymmetric *P*1 space group, which is frequently encountered among mechanoluminescent organic materials. Therefore, the crystals were additionally tested for a possible mechanoluminescent response by gentle grinding between two glass slides in the dark. Under mechanical stimulation, visible emission was indeed observed (Video S1, Supporting Information).

In the case of compound **4**, the asymmetric part of the unit cell contains half of the anhydride molecule and half of a disordered cyclohexane molecule, refined in two positions (Figure S10 in the Supporting Information). The *tert*-butyl groups are disordered and refined into two positions. As in other crystals, the primary intermolecular interactions in crystal **4** are C−H···π interactions (Figure S11 in the Supporting Information). Cyclohexane molecules form hydrogen bonds with oxygen atoms. Geometric parameters of intermolecular interactions are presented in Table S6 in the Supporting Information.

The thermal stability of dyes **1**−**4** was evaluated by thermogravimetric analysis (TGA) (Figure S12 in the Supporting Information), with the results summarized in Table S7, Supporting Information. All compounds exhibited moderate temperatures for 5% weight loss (T_d), ranging from 196 to

https://doi.org/10.1021/acsami.6c11053
ACS Appl. Mater. Interfaces XXXX, XXX, XXX−XXX

335 °C. Interestingly, the *para*-substituted derivatives **1** and **2** showed higher T_d values than their *ortho*-substituted counterparts **3** and **4**, likely due to steric hindrance in the latter. Differential scanning calorimetry (DSC) was employed to study the morphological transitions of the synthesized compounds. Compounds **1** and **3**, featuring unsubstituted carbazole donors, were isolated after synthesis and purification as crystalline materials, as confirmed by DSC (Figure S13, Supporting Information). Sharp endothermic melting effects (T_m) were observed in the first heating scans at 257 and 161 °C, respectively (Table S7, Supporting Information). In subsequent cooling scans, no crystallization peaks were observed for either of the compounds. In the second heating scan, only glass transition signals (T_g) were observed for compounds **1** and **3** at 96 and 67 °C, respectively (Table S7, Supporting Information). In contrast, compounds **2** and **4**, containing 3,6-di-*tert*-butylcarbazole units, were obtained as amorphous materials. Peaks due to crystallization or melting did not appear in cooling and heating cycles between 0 °C and 300 °C. The glass-transition temperatures obtained from the repeated heating scans of compounds **2** and **4** were 126 and 115 °C, respectively. This amorphous nature likely explains why we could not obtain suitable single crystals for SCXRD analysis from compound **2**, whereas crystals of dye **4** were successfully grown as a cyclohexane solvate. It should be noted that dyes **2** and **4**, containing 3,6-di-*tert*-butylcarbazole donors, exhibited higher glass transition temperatures (T_g) of 126 and 115 °C, respectively, compared to their unsubstituted carbazole counterparts **1** and **3**, which showed T_g values of 96 and 67 °C, respectively. This behavior can likely be attributed to the presence of the *tert*-butyl groups, which introduce significant steric hindrance, restrict molecular mobility, and reduce the efficiency of molecular packing, thereby suppressing crystallization and enhancing the amorphous character of the materials.

Electrochemical Properties

Cyclic voltammetry (CV) was employed to determine the ionization energies (IEs) and electron affinities (EAs), which are key electronic parameters for materials used in OLEDs. The CV curves recorded for solutions of the compounds in anhydrous dichloromethane (DCM) are presented in Figure S14 in the Supporting Information. Both positive and negative potential scans were performed to probe the redox behavior of the synthesized compounds and to estimate their frontier energy levels. The observation of both oxidation and reduction processes in the CV traces indicates the bipolar electrochemical behavior of all the investigated compounds. The IE and EA values were estimated from the onset potentials of oxidation and reduction, respectively (Table S8 in the Supporting Information). All redox potentials were referenced to the ferrocene/ferrocenium (Fc/Fc^+) redox couple.

The IE values of the investigated compounds fall in the range of 5.53−5.74 eV. The highest ionization energy (5.74 eV) was observed for compound **1**, which contains unsubstituted carbazole donor moieties and a *para*-substituted benzoic anhydride core. The lowest IE value (5.53 eV) was obtained for compound **4**, incorporating 3,6-di-*tert*-butylcarbazole donor fragments and an *ortho*-substitution pattern relative to the benzoic anhydride unit. Compounds **2** (IE = 5.62 eV) and **4**, bearing 3,6-di-*tert*-butylcarbazole donor units, exhibit lower IE values than their counterparts **1** (IE = 5.74 eV) and **3** (IE = 5.66 eV), which contain unsubstituted carbazole donors. In addition, the further decrease in IE is observed when moving from the *para*-linked derivatives (**1** and **2**) to the corresponding *ortho*-linked analogues (**3** and **4**). Both trends are in good agreement with the results of theoretical calculations (see next chapter). The lower ionization energies can be attributed to the stronger electron-donating character of 3,6-di-*tert*-butylcarbazole relative to unsubstituted carbazole, as well as to the reduced conjugation between the donor and acceptor units in the *ortho*-linked derivatives. The latter effect destabilizes the HOMO, leading to a reduction in the ionization energy.

The EA values of compounds **1**−**4** fall within a narrow range of 2.79−2.89 eV. This observation is consistent with the theoretical calculations, which show that the LUMO is predominantly localized on the benzoic anhydride moiety, a structural feature common to all four compounds. Consequently, the reduction process is largely insensitive to both the donor strength and the substitution pattern of the investigated derivatives.

Quantum Chemical Calculations

Time-dependent density functional theory (TD-DFT) calculations were performed for compounds **1**−**4** to gain insight into their electronic structures and excited-state properties (Table S9 in the Supporting Information). For all four synthesized compounds, the LUMO is predominantly localized on the electron-accepting benzoic anhydride moiety. In compounds **3** and **4**, in which the carbazole donor units are connected to the acceptor through *ortho*-positions, steric hindrance results in pronounced localization of the HOMO on a single carbazole unit, with only minor delocalization onto the adjacent phenyl ring of the acceptor. This enhanced spatial separation of the frontier molecular orbitals leads to very small calculated ΔE_{ST} of 0.08 and 0.09 eV for compounds **3** and **4**, respectively.

In contrast, in compounds **1** and **2**, where the donor and acceptor units are connected through the *para*-positions, the HOMO remains primarily localized on the carbazole donors but exhibits greater delocalization over the molecular backbone. Consequently, the calculated ΔE_{ST} values for compounds **1** and **2** are larger, amounting to 0.28 and 0.29 eV, respectively, than those of their *ortho*-substituted analogues.

Overall, the theoretical calculations predict relatively small S_1-T_1 energy gaps for all synthesized anhydrides, especially compounds **3** and **4**, suggesting that these compounds are promising candidates for exhibiting TADF.

Photophysical Properties

Solutions and Non-doped Films. The UV−Vis absorption spectra of dilute solutions of dyes **1**−**4** (e.g., toluene, $2.0 \cdot 10^{-5}$ M) were recorded, revealing structured $\pi \rightarrow \pi^*$ transitions in the 300−400 nm range (Figure 2a and Figure S15 and Table S10 in the Supporting Information). Absorption peaks at ca. 325 nm and 340 nm are typically attributed to $\pi \rightarrow \pi^*$ transitions of carbazole units. The slight solvent-dependent shifts of the peak positions suggest that the excited states have a predominantly locally excited (LE) character with a small contribution from charge transfer (CT).

In the absorption spectra of the solutions of dyes **1**−**4**, the lowest-energy band (LEB) corresponds to a CT transition from the donor carbazole moieties to the acceptor benzoic anhydride unit. In the spectra of toluene solutions (Figure 2a), the LEB appears as a broadened tail extending from 360 to 400 nm. With the increase of the solvent polarity, bathochromic (red)

https://doi.org/10.1021/acsami.6c11053
ACS Appl. Mater. Interfaces XXXX, XXX, XXX−XXX

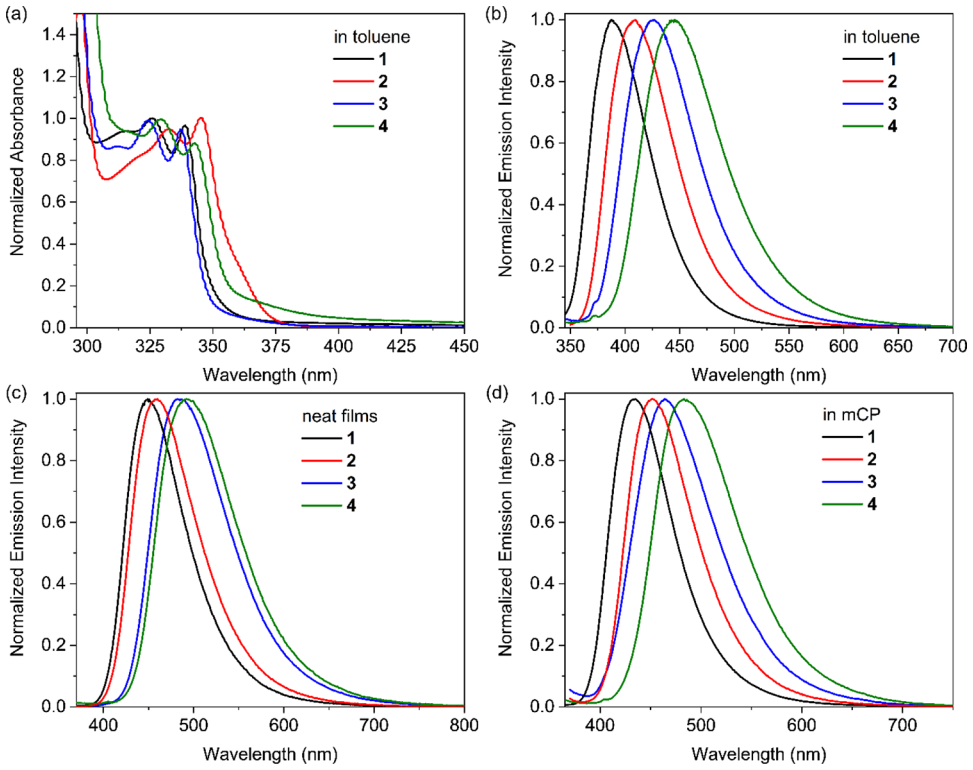

Figure 2. Normalized absorption (a) and photoluminescence (b) spectra of the solutions of dyes **1**−**4** in toluene ($C = 2.0 \cdot 10^{-5}$ M, $\lambda_{ex} = 335$ nm). Normalized photoluminescence spectra of non-doped thin films (c) and thin films of the dyes dispersed in mCP (10 wt % of the dye) (d) of dyes **1**−**4** ($\lambda_{ex} = 335$ nm).

shifts of the LEB absorption bands were observed for the solutions of compounds **3** and **4**, accompanied by an increase in absorbance. This observation indicates stabilization of the excited states relative to the ground states and suggests a significant intramolecular charge transfer (ICT) character of the electronic transitions.

Photoluminescence (PL) spectra of the dilute solutions of solvents with varying polarity, including toluene, chloroform, dichloromethane, acetone, and acetonitrile, were recorded in order to investigate solvent-dependent emission. Steady-state PL spectra were taken under excitation at 335 nm. Absolute photoluminescence quantum yields (PLQYs) were determined using an integrating sphere. Normalized PL spectra of the toluene solutions of compounds **1**−**4** are presented in Figure 2b. The solution of compound **1**, featuring a *para*-linked donor–acceptor substitution pattern, exhibits emission maximum at 392 nm with a PLQY of 0.36. Replacement of carbazole fragment by the stronger donor 3,6-di-*tert*-butylcarbazole fragment (compound **2**) results in the bathochromic shift of the emission maximum to 407 nm and PLQY of 0.29. For the solution of compound **3**, in which the carbazole units are linked to benzoic anhydride moiety through the *ortho*-position, the emission maximum is further red-shifted to 425 nm with a PLQY of 0.07. Replacing the carbazole donor in compound **3** with 3,6-di-*tert*-butylcarbazole fragment (compound **4**) leads to the additional bathochromic shift to 443 nm and PLQY of 0.10. These findings are in good agreement with the results of theoretical calculations, which predict significantly smaller band gaps for compounds **3** and **4** compared to compounds **1** and **2**. The introduction of the stronger donor 3,6-di-*tert*-butylcarbazole consistently results in a bathochromic shift of the emission maximum by 15−18 nm.

In general, PL spectra of the solutions of the synthesized compounds are characterized by unstructured single emission bands. The PL spectra of all the compounds exhibit positive solvatochromism, with PL maxima shifting bathochromically as solvent polarity increases from that of toluene to that of acetonitrile (Figure S15 and Table S10 in the Supporting Information). The highest PL quantum yields were observed for the solution of compound **1** in chloroform (PLQY = 0.47). This trend is consistent across compounds **1**−**4**, with the highest PLQY values estimated for the solutions in chlorinated solvents such as chloroform and dichloromethane. The lowest PL quantum yields were observed for acetonitrile solutions. Comparison of PLQY values of the solutions reveals that compounds **1** and **2** with *para*-linkage exhibit PL quantum yields by a factor of ca four higher than compounds **3** and **4** with *ortho*-linkage.

We also studied the photophysical properties of non-doped thin films of compounds **1**−**4**. The photoluminescence spectra of non-doped films exhibit a pronounced blue shift relative to those recorded for the solutions in polar solvents (Figure 2c and Table 1). This observation can be attributed to the sensitivity of the ICT excited state to the polarity of the surrounding medium. In polar solvents such as chloroform, acetone, and dichloromethane, the CT state is more strongly stabilized, leading to the decrease of its energy and a corresponding bathochromic (red) shift of the emission.

In contrast, the PL spectra of the solutions of the compounds in non-polar toluene are blue-shifted with respect to those of the non-doped films, owing to the low polarity of toluene, which provides minimal stabilization of the polar CT state. In the solid state, however, the intermolecular interactions and heterogeneous

https://doi.org/10.1021/acsami.6c11053
ACS Appl. Mater. Interfaces XXXX, XXX, XXX−XXX

local microenvironments can partially stabilize the CT state, resulting in a red shift of the emission relative to that of toluene solution (approximately by 50 nm). Conformational restrictions in the solid film may favor more stabilized emissive geometries, contributing to the observed spectral shifts.

The PLQY values of the solutions of the compounds in toluene were in the range of 0.07−0.36, with the highest PLQY observed for the solution of dye **1** (Table S10 in the Supporting Information). The PLQY values of the solid samples were higher, ranging from 0.19 to 0.37 (Table 1), compared to those measured for toluene solutions. This is most clearly evident for compounds **3** and **4**. The PL quantum yields of the solid samples of these compounds are by 2−3 times higher than those of the solutions. This behavior is indicative of aggregation-induced emission enhancement (AIEE), a phenomenon commonly observed in *ortho*-phenylene-linked donor−acceptor systems.[39,42] The enhanced emission is attributed to the restriction of intramolecular motions in the aggregated state, which reduces the reorganization of the excited-state geometry and suppresses non-radiative relaxation pathways, thereby increasing the radiative decay efficiency.

The emission lifetimes of non-doped films of compounds **1** and **2** are in the nanosecond range, whereas the corresponding films of *ortho*-analogues **3** and **4** exhibit both nanosecond- and microsecond-lived emission components (Table S11 and Figure S16 in the Supporting Information). This behavior suggests the presence of an additional long-lived emissive process in the *ortho*-substituted compounds.

Host−Guest Systems. The photophysical properties of emitter−host blends containing 5−20 wt % emitter (in 5 wt % increments) in the commercially available host 1,3-bis(*N*-carbazolyl)benzene (mCP) were investigated to evaluate the efficiency of energy transfer to the emitters. The normalized PL spectra of mCP films doped with dyes **1**−**4** at different concentrations are presented in Figure 2d and Figure S17 and Table S12 Supporting Information. As the emitter concentration in the mCP host increases from 5 to 20 wt %, the PL maxima exhibit slight bathochromic shifts. The shifts are approximately 5 nm for dyes **2**−**4** and up to 15 nm for dye **1**. Such red shifts are commonly attributed to enhanced intermolecular interactions at higher dopant concentrations, which may promote the formation of molecular aggregates or excimers.

Blends containing 5 and 10 wt % of dyes **2** and **4** in the mCP host exhibit the highest PLQYs, reaching 0.47−0.60 for the blends containing dye **2** and approximately 0.40 for those containing dye **4** (Table 1). These values are more than twice as high as those measured for the corresponding non-doped films, indicating efficient Förster resonance energy transfer (FRET) in the host−guest systems. The PLQY of the film of dye **1** dispersed in mCP is comparable to that of the corresponding non-doped film. This observation can be rationalized by the intrinsically high luminescence efficiency of dye **1** in the solid state, for which incorporation into a host matrix does not provide additional benefits, such as suppression of aggregation-caused quenching, enhanced energy transfer, or reduced nonradiative losses. In contrast, incorporation of dye **3** into the mCP matrix generally results in lower PLQYs compared with the non-doped film, although the PLQY shows an increasing trend with increasing dopant concentration.

Then, considering the ability of the *ortho*-substituted anhydrides to exhibit long-lived emission (see the previous section), the photoluminescence decay dynamics of the corresponding host−guest films were investigated. Host−guest films containing compounds **3** and **4** dispersed in mCP (10 wt % emitter) were fabricated by vacuum deposition. PL decay curves were recorded at different temperatures (Figure S18 in the Supporting Information). Three different temporal windows were selected to predominantly capture prompt fluorescence (PF) within 200 ns after excitation, TADF within 50 μs after excitation, and RTP within 10 ms after excitation. These measurements enabled the determination of emission lifetimes and the relative contributions of PF, TADF, and RTP at different temperatures, as described in the Supporting Information (Section 5.1 Determination of kinetic parameters, Tables S13−S15).

Table 1. Photophysical Properties of Non-doped Thin Films of 1−4 and of Thin Films of the Dyes Doped in mCP (10 wt % of Dye)

dye	sample	λ_{PL} (nm)	PLQY
1	nondoped film	448	0.37
2	nondoped film	460	0.20
3	nondoped film	485	0.29
4	nondoped film	492	0.19
1	in mCP	425	0.39
2	in mCP	448	0.60
3	in mCP	461	0.18
4	in mCP	480	0.40

The PF decay intensities remained nearly unchanged over the investigated temperature range. In contrast, the TADF decay intensity increased, whereas the RTP intensity decreased with increasing temperature for both compounds. Compound **4** showed higher ISC and RISC rate constants (3.79×10^7 s^{-1} and 2.59×10^4 s^{-1}, respectively) than compound **3** (1.26×10^6 s^{-1} and 2.99×10^3 s^{-1}, respectively). This difference is consistent with the smaller ΔE_{ST} value of compound **4** (0.05 eV) compared with compound **3** (0.08 eV) (Figure S22 in the Supporting Information). Moreover, anhydride **4** exhibited faster triplet-state emissive relaxation, with a rate constant of 1.13×10^3 s^{-1}, compared with 1.19×10^2 s^{-1} for compound **3.**

To further elucidate the excited-state relaxation processes, time-resolved photoluminescence (TRPL) spectroscopy was performed on the mCP host−guest systems containing compounds **3** and **4** (Figure 3). The time-resolved emission spectra reveal a distinct temporal evolution of the emissive states. For both emitters, the intense short-lived emission observed within the first few microseconds is attributed to PF together with the TADF component.

At longer delay times (>15 μs), the emission progressively shifts toward lower energies (490−550 nm), and the spectra become broader, indicating an increasing contribution from long-lived triplet-derived emission, including TADF and RTP.[8,44] Comparison of the normalized spectra recorded at 2.5 μs and 47 μs clearly demonstrates the evolution of the emissive state: the early-time spectrum is dominated by higher-energy PF/TADF emission, whereas the later-time spectrum is governed by emission from the more stabilized triplet excited states. These findings confirm that both compounds exhibit dual TADF/RTP emission when molecularly dispersed in the mCP matrix.

Electroluminescence Properties

To evaluate the electroluminescent (EL) performance, vacuum-deposited hosts-containing OLEDs were fabricated using a simple multilayer architecture: indium tin oxide (ITO)/CuI

https://doi.org/10.1021/acsami.6c11053
ACS Appl. Mater. Interfaces XXXX, XXX, XXX−XXX

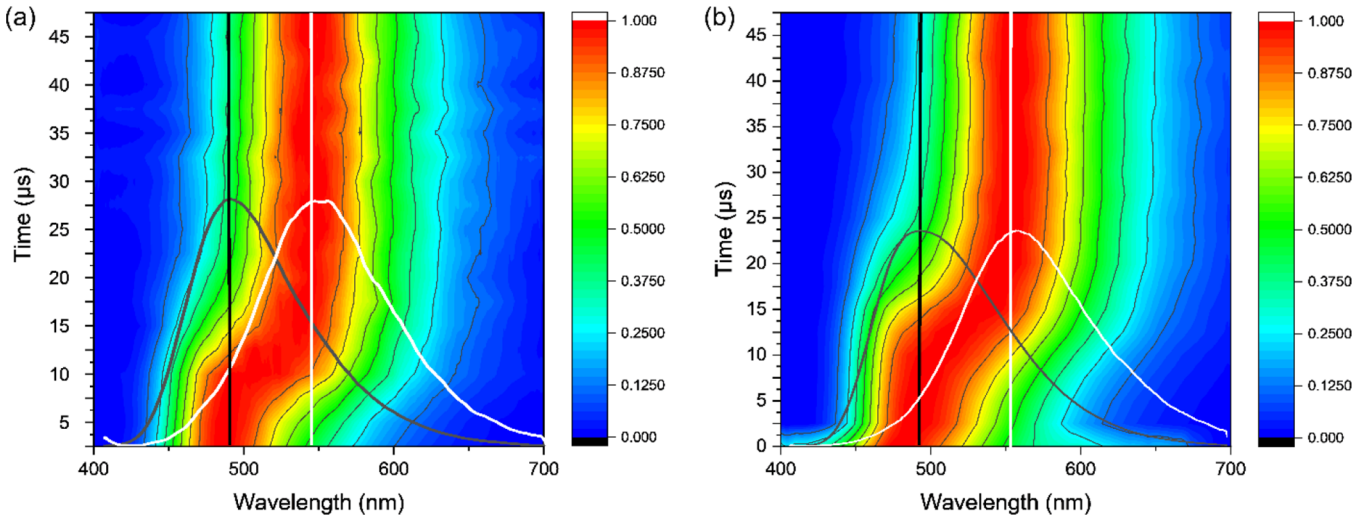

Figure 3. Time-resolved emission spectra of the mCP based host−guest system with compounds **3** (a) and **4** (b). Colors from red to blue represent the PL intensity from high to low. The change of the normalized spectra at different time.

(5 nm)/*N*,*N*′-bis(3-methylphenyl)-*N*,*N*′-diphenylbenzidine (TPD, 50 nm)/1,3-bis(*N*-carbazolyl)benzene (mCP):10 wt % of emitter **3** or **4** (light-emitting layer, EML, 20 nm)/diphenyl[4-(triphenylsilyl)phenyl]phosphine oxide (TSPO1, 5 nm)/2,2′,2″-(1,3,5-benzenetriyl)tris(1-phenyl-1*H*-benzimidazole) (TPBi, 40 nm)/Ca (50 nm)/Al (200 nm) (Figure 4). In this configuration, the films of compounds **3** and **4** doped in mCP serve as the EMLs. CuI and TPD ensure efficient hole injection and transport, while TSPO1 and TPBi provide effective exciton confinement and electron transport, respectively; the Ca/Al bilayer acts as a cathode.

OLEDs based on compounds **3** and **4** exhibit turn-on voltages of 5.0 V and 5.5 V, respectively, and generate intense sky-blue EL peaking at 475 nm and 481 nm, respectively (Figure 4). The EL spectra closely match the photoluminescence spectra of the corresponding films of the compounds dispersed in mCP, indicating that emission originates predominantly from the anhydrides rather than from the host matrix. Importantly, due to the small singlet−triplet energy gaps of these compounds the observed EL arises from triplet exciton utilization via TADF/RTP. The minor differences between PL and EL spectra are attributed to charge recombination dynamics, interfacial exciton formation, and interactions with the charge-transporting layers under electrical excitation.

The TADF/RTP-based OLEDs exhibit outstanding electroluminescent performance, combining exceptionally high luminance with high efficiency. The maximum luminance values reach 62 000 cd m^{-2} for the device based on compound **4** and 39 000 cd m^{-2} for that based on compound **3**, demonstrating the ability of these emitters to sustain efficient electroluminescence under intense electrical excitation. Notably, the device employing compound **4** achieves a maximum current efficiency (CE) of 39.0 cd A^{-1}, power efficiency (PE) of 11.0 lm W^{-1}, and external quantum efficiency (EQE) of 21.0%, substantially surpassing the performance of the device based on compound **3** (CE = 25.0 cd A^{-1}, PE = 8.0 lm W^{-1}, EQE = 13.7%) (Figure 4 and Table 2). Such a combination of high luminance and high efficiencies are particularly remarkable for purely organic TADF/RTP emitters, underscoring the effectiveness of triplet exciton confinement and radiative decay in these anhydride-based systems. It should be noted that the high EQE values result not only from efficient exciton utilization but also from favorable optical properties of the emitting layers. An ideal Lambertian emitter exhibits an angular emission intensity proportional to cos θ, leading to a characteristic angular intensity distribution. In contrast, the measured angular photoluminescence profiles of the emitting layers deviate from the Lambertian emission profile (Figure S23 in the Supporting Information), indicating enhanced light extraction from the OLED structure. Optical simulations further confirm improved light-outcoupling efficiency in the investigated devices (Figure S23 in the Supporting Information). These optical effects contribute to the high EQEs observed for the developed OLEDs.

Furthermore, both devices demonstrate remarkably stable EQE over a wide luminance range (Figure 4d), indicating a strongly suppressed efficiency roll-off, which remains one of the major challenges for triplet-emitting OLEDs. Even at a high luminance of 30 000 cd m^{-2}, the EQE is maintained at 19% for the device based on compound **4** and 11% for that incorporating compound **3**, highlighting the excellent operational stability of these emitters under high current densities.

The small EQE roll-off can be attributed to the unique excited-state relaxation pathways of compounds **3** and **4**, which combine TADF with RTP. The coexistence of these two emissive channels enables efficient utilization of electrically generated triplet excitons while reducing their accumulation within the emissive layer. In particular, the relatively fast RISC process continuously converts triplet excitons into emissive singlet states, whereas the RTP channel provides an additional radiative relaxation pathway for triplets that are not harvested through the TADF mechanism. As a result, the steady-state triplet exciton population is effectively reduced, suppressing exciton-induced quenching processes that are primarily responsible for efficiency losses at high brightness.

The favorable photophysical properties of the emitters are further complemented by the optimized device architecture. The high-triplet-energy mCP host effectively confines excitons within the emitting layer while facilitating efficient energy transfer to the guest molecules. At the same time, the charge-transporting layers promote balanced hole and electron injection, minimizing charge accumulation and broadening of the recombination zone.

https://doi.org/10.1021/acsami.6c11053
ACS Appl. Mater. Interfaces XXXX, XXX, XXX−XXX

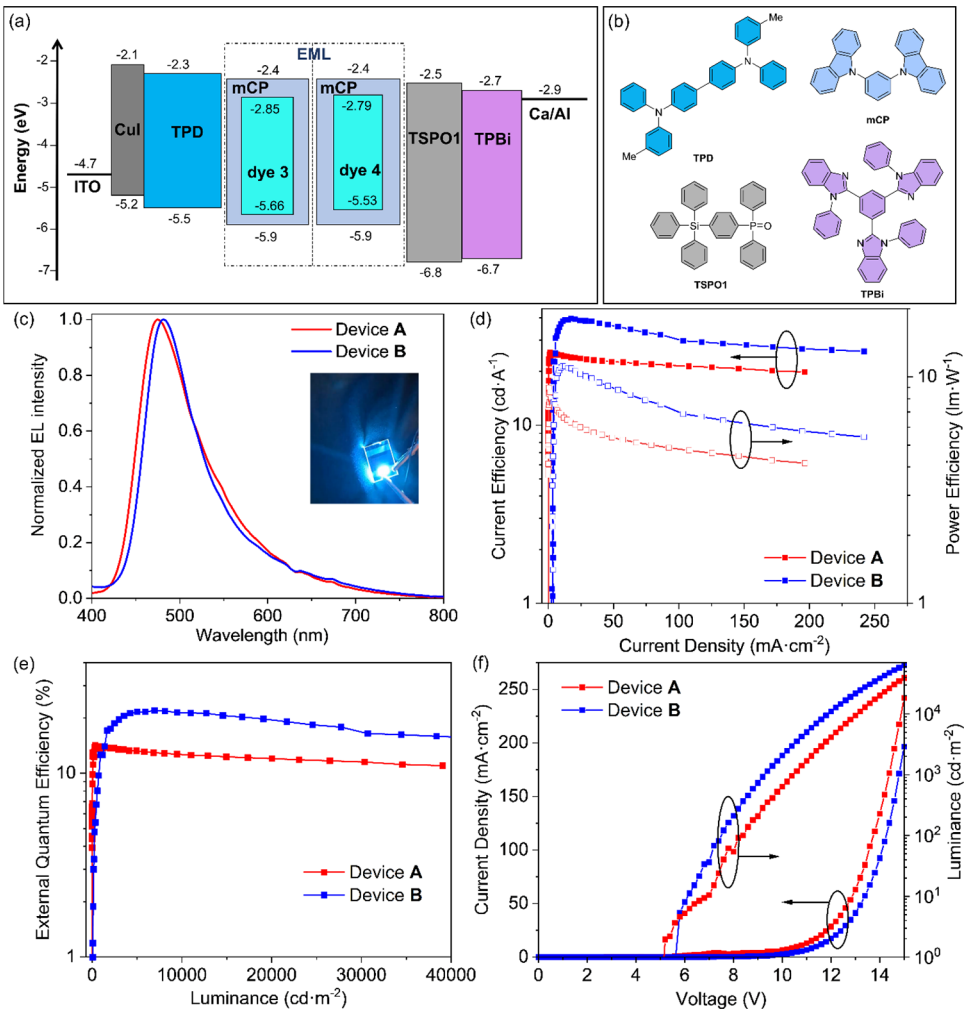

Figure 4. Electroluminescence properties of OLEDs with emitting layers of compounds **3** and **4** dispersed in mCP: schematic representation of the device architecture with the energy-levels (a); the chemical structures of semiconductor materials (b); EL spectra of OLEDs (c); current and power efficiency versus current density (d); external quantum efficiency versus luminance (e); and current density and luminance versus voltage plots (f).

Table 2. Characteristics of OLEDs Based on Emitters 3 and 4

device	Emitter	λ_{EL} [a] (nm)	V_{on} [b] (V)	L [c] (cd·m^{-2})	CE [d] (cd·A^{-1})	PE [e] (lm·W^{-1})	EQE [f] (%)	CIE [g]
A	**3**	475	5.0	39000	25.0/24.8/23.0	8.0/7.3/5.5	13.7/13.5/12.6	(0.22; 0.38)
B	**4**	481	5.5	62000	39.0/31.5/38.4	11.0/9.9/10.0	21.0/12.6/21.4	(0.23; 0.38)

[a]Wavelengths of EL intensity maxima. [b]Turn-on voltage at 10 cd·m^{-2}. [c]Maximum luminance. [d]Maximum current efficiency and current efficiency at 1000 cd·m^{-2}, and 10,000 cd·m^{-2}. [e]Maximum power efficiency and power efficiency at 1000 cd·m^{-2}, and 10,000 cd·m^{-2}. [f]Maximum external quantum efficiency and external quantum efficiency at 1000 cd·m^{-2}, and at 10,000 cd·m^{-2}. [g]Commission Internationale de l'Éclairage color coordinates at 1000 cd·m^{-2}.

Collectively, these factors reduce the probability of bimolecular quenching processes, including triplet−triplet annihilation and triplet−polaron annihilation, thereby contributing to the exceptionally small EQE roll-off observed in the developed devices.

The corresponding CIE 1931 color coordinates of (0.22, 0.38) for the device based on compound **3** and (0.23, 0.38) for the device based on compound **4** confirm their sky-blue electroluminescence (Table 2). Moreover, the EL spectra remain essentially unchanged with increasing driving voltage (Figure S24 in the Supporting Information), indicating stable exciton recombination and the absence of field-induced spectral shifts or excimer formation.

Collectively, these results demonstrate that the proposed anhydride-based emitters, combining TADF and RTP emission within a single molecular framework, provide an effective strategy for efficient triplet harvesting in OLEDs. Unlike conventional TADF emitters, which rely exclusively on reverse intersystem crossing, these materials exploit an additional RTP relaxation pathway that facilitates efficient triplet depopulation under electrical excitation. This dual-emission mechanism, together with the optimized host−guest architecture, enables the simultaneous realization of high luminance, high electroluminescence efficiency, excellent color stability, and remarkably low efficiency roll-off, making these emitters

https://doi.org/10.1021/acsami.6c11053
ACS Appl. Mater. Interfaces XXXX, XXX, XXX−XXX

promising alternatives to both purely organic TADF materials and heavy-metal phosphorescent complexes for the development of high-brightness OLEDs.

■ CONCLUSIONS

We have developed a simple and efficient synthetic approach for the preparation of C_2-symmetric anhydrides (**1**–**4**) derived from carbazole-based benzoic acids featuring a donor–acceptor–donor architecture. The study of photophysical studies revealed a pronounced structure–property relationship. Compounds **3** and **4**, bearing *ortho*-linked carbazole donor moieties, exhibit small singlet–triplet energy gaps. Dyes **3** and **4** exhibit both TADF and room temperature phosphorescence. Compounds **1** and **2**, with *para*-linked donor–acceptor motifs, show neither delayed fluorescence nor phosphorescence. Owing to their favorable emissive properties, compounds **3** and **4** were successfully employed as emitters in sky-blue OLEDs. The resulting OLEDs demonstrated electroluminescence maxima at 475 and 481 nm, with impressive maximum external quantum efficiencies of 13.7% and 21.0%, respectively. In addition, high maximum luminance values of 39 000 cd m^{-2} and 62 000 cd m^{-2}, along with low efficiency roll-off, were achieved.

Taking into account these outstanding device characteristics, we believe that the proposed design strategy based on the straightforward conversion of aromatic acids into emissive anhydrides exhibiting TADF and RTP simultaneously can be readily extended to a broad range of mono- or multidonor-substituted aromatic and heterocyclic acids. Furthermore, the systematic variation of donor strength and acceptor linkage offers a versatile platform for tuning emission across a wide spectral range, paving the way toward the development of emitters for highly efficient multicolor OLEDs.

■ EXPERIMENTAL SECTION

1. General Remarks

Materials. All reagents and chemicals were purchased from commercial sources (TCI, Acros Organics, FluoroChem) and used without further purification. Synthesized compounds were purified via flash column chromatography on silica gel (Merck, 230–400 mesh). Reactions progress was controlled by thin layer chromatography (TLC), carried out on commercially available aluminum plates covered with silica gel (60 F_{254}, Merck) plates and visualized using a laboratory UV lamp.

Instrumental Methods

Structural Characterisation. NMR spectra were recorded at room temperature using Varian Mercury 400 MHz (400 MHz for ^{1}H and 100 MHz for ^{13}C NMR spectra) or Varian V NMRS 500 MHz (500 MHz for ^{1}H and 125 MHz for ^{13}C NMR spectra) spectrometers. $CDCl_3$ or DMSO-d_6 was used as the solvent, and chemical shifts were referenced to solvent peaks.[45] Signal multiplicities are reported as "s", "d", "dd", "ddd", "t", "td", and "m", corresponding to singlet, doublet, doublet of doublets, doublet of doublets of doublets, triplet, triplet of doublets, and multiplet, respectively. Data was processed using MestReNova software. High-resolution mass spectra (HRMS) were collected on a Synapt G2-S HDMS (Waters Inc.) mass spectrometer equipped with an atmospheric-pressure chemical ionization (APCI) ion source or electrospray ionization (ESI) ion source and quadrupole-Time-of-Flight (q-TOF) mass analyzer. The instrument was controlled and recorded data were processed using MassLynx V4.1 software package (Waters Inc). Spectra were collected in ESI or APCI mode.

Single crystals of dye **3** were grown by recrystallization from hexanes-toluene mixture. Crystals of anhydride **1** were obtained by slow evaporation from hexanes-chloroform mixtures, while crystals of dye **4** were obtained by recrystallization from cyclohexane. SCXRD measurements were performed at 100 K (crystals of compounds **1** and **3**) and 250 K (crystal of compound **4**; due to the phase transition occurring below 250 K leading to the lower-symmetry twin) using the Rigaku XtaLAB Synergy-DW diffractometer equipped with the HyPix-Arc 150° detector using Cu Kα radiation (λ = 1.5418 Å) and the Oxford Cryosystems Cryostream 800 Plus for sample temperature control. Data reduction, scaling, analysis and numerical (analytical) absorption corrections were carried out using the CrysAlisPro[46] software. The SHELXT[47] and SHELXL[48] programs (implemented in the Olex2[49] program) were used to solve and refine the crystal structures. All non-hydrogen atoms were refined anisotropically with full-matrix least-squares techniques on F^2. Hydrogen atoms were located in difference Fourier maps and then refined with geometric restraints. Experimental and crystallographic details are given in Tables S1–S3.

Theoretical calculations of the dyes **1**–**4** were performed using density-functional theory via Spartan'14 software package. Differential scanning calorimetry (DSC) measurements were done with a TA Instruments "DSC Q100" calorimeter. The samples were heated at a scan rate of 10 °C·min^{-1} under nitrogen atmosphere. Thermogravimetric analysis (TGA) was performed on a "Mettler TGA/SDTA851e/LF/1100" at a heating rate of 20 °C/min under nitrogen atmosphere.

Electrochemical measurements were done using μAutolab Type III (EcoChemie, Netherlands) potentiostat, glassy carbon electrode (diam. 2 mm), platinum coil and silver wire as working, auxiliary and reference electrode, respectively and the scan rate of 2.5 mV·s^{-1} with concentration of compounds $1.0 \cdot 10^{-4}$ M. Potentials are referenced with respect to ferrocene (Fc), which was used as the internal standard. Cyclic voltammetry (CV) experiments were conducted in the dry solvent solution containing 0.1 M tetrabutylammonium hexafluorophosphate ($TBAPF_6$) as the electrolyte at room temperature under nitrogen atmosphere. For all synthesized compounds, measurements were done in DCM solution. Deaeration of the solution was achieved by a nitrogen bubbling for about 10 min before measurement.

Photophysics. UV–vis spectra in solutions were recorded on a Shimadzu UV-3600i Plus spectrophotometer at room temperature. Steady-state fluorescence emission spectra were performed at room temperature on an Edinburgh Instruments Spectrophotometer (FS5, Edinburgh, UK) with xenon lamp as the light source. The absolute fluorescence quantum yields were measured with a calibrated SC-30 Integrating Sphere and were excited at the appropriate absorption wavelength in each case. Fluorescence decays of the solutions and solid-state samples were measured using a pulsed diode laser (PDL 820, PicoQuant, λ_{ex} = 374 nm) integrated into an Edinburgh Instruments FLS980 spectrometer. Decay curves at various temperatures were recorded under deoxygenated conditions using an Optistat DN2 cryostat coupled with a turbomolecular pump.

OLEDs were formed by thermal deposition in a vacuum (10^{-5} Torr) on a glass substrate with a transparent conductive layer of ITO, by stepwise deposition of a hole–injection layer of CuI, hole-transporting layer (TPD) along with an electron-transporting layer (TPBi). Compounds **3** and **4** were doped in mCP, and the mCP:**3** and mCP:**4** layers were formed by controlled simultaneous deposition from two sources. Calcium and aluminum were used as cathode materials with a low work function, providing good electron injection to the electron-transport layer. The active area of the obtained devices was 6 mm^2. The density–voltage and luminance–-voltage characteristics were measured by using a semiconductor parameter analyzer HP4145A. The measurement of brightness was obtained using a calibrated photodiode, and the electroluminescence spectra were recorded with an Ocean Optics USB2000 spectrometer.

Synthesis

Ethyl 4-(9*H*-carbazol-9-yl)benzoate (**9**), ethyl 4-(3,6-di-*tert*-butyl-9*H*-carbazol-9-yl)benzoate (**10**), 4-(9*H*-carbazol-9-yl)benzoic acid (**13**), 4-(3,6-di-*tert*-butyl-9*H*-carbazol-9-yl)benzoic acid (**14**),[41] as well as

https://doi.org/10.1021/acsami.6c11053
ACS Appl. Mater. Interfaces XXXX, XXX, XXX–XXX

methyl 2-(9*H*-carbazol-9-yl)benzoate (**11**) and 2-(9*H*-carbazol-9-yl)benzoic acid (**15**)[42] were synthesized as described previously.

Methyl 2-(3,6-di-*tert*-butyl-9*H*-carbazol-9-yl)benzoate (**12**) was synthesized using a modified literature procedure.[50] The mixture of methyl 2-iodobenzoate (**8**, 1.27 g, 4.84 mmol, 1.1 equiv), 3,6-di-*tert*-butyl-9*H*-carbazole (**6**, 1.23 g, 4.40 mmol, 1.0 equiv), potassium carbonate (1.81 g, 13.21 mmol, 3.0 equiv), copper (I) iodide (84 mg, 0.44 mmol, 0.1 equiv), and 1,10-phenanthroline (79 mg, 0.44 mmol, 0.1 equiv) in dimethylacetamide (10 mL) was refluxed for 24 h under argon. After cooling, the mixture was filtered through silica gel, eluting with hexanes/ethyl acetate (8:1), and concentrated. The residue was separated by column chromatography on silica gel (hexanes, next hexanes/AcOEt = 98:2) to afford pure product **12** (1.42 g, 3.43 mmol, 78%) as a white powder. ^{1}H NMR (500 MHz, $CDCl_3$) δ = 8.15 (d, *J* = 1.8 Hz, 2H), 8.09 (m, 1H), 7.73 (dd, *J* = 7.6 Hz, *J* = 1.4 Hz, 1H), 7.54−7.59 (m, 2H), 7.43 (dd, *J* = 8.6 Hz, *J* = 1.8 Hz, 2H), 7.07 (d, *J* = 8.6 Hz, 2H), 3.24 (s, 3H), 1.47 (s, 18H) ppm. ^{13}C{H} NMR (126 MHz, $CDCl_3$) δ = 166.69, 142.59 (2C), 140.00 (2C), 137.46, 133.16, 131.77, 129.89, 129.84, 127.80, 123.57 (2C), 123.26 (2C), 116.21 (2C), 108.65 (2C), 52.07, 34.68 (2C), 32.00 (6C) ppm. HRMS (ESI-TOF) calculated for $C_{28}H_{31}NO_2Na$ $[M + Na]^+$: 436.2252, found: 436.2259.

2-(3,6-Di-*tert*-butyl-9*H*-carbazol-9-yl)benzoic acid (**16**). The mixture of ester **12** (1.20 g, 2.90 mmol, 1.0 equiv), tetrahydrofuran (15 mL), ethanol (5 mL), water (5 mL) and KOH (0.49 g, 8.70 mmol, 3.0 equiv) was refluxed for 12 h, and then cooled to room temperature. The solvents were evaporated and water (5 mL) and 5N HCl aqueous solution were slowly added to pH ∼ 5. The mixture was left in a fridge for 3 h. The formed precipitate was filtered, washed with water and dried to give acid **16** (1.16 g, ∼100%) as a white powder. ^{1}H NMR (400 MHz, DMSO-d_6) δ = 8.18 (d, *J* = 1.7 Hz, 2H), 7.81 (dd, *J* = 7.2 Hz, *J* = 2.0 Hz, 1H), 7.42−7.52 (m, 2H), 7.37 (dd, *J* = 8.6 Hz, *J* = 1.9 Hz, 2H), 7.27 (dd, *J* = 7.4 Hz, *J* = 1.4 Hz, 1H), 7.02 (d, *J* = 8.6 Hz, 2H), 1.42 (s, 18H) ppm. ^{13}C{H} NMR (101 MHz, DMSO-d_6) δ = 169.02, 141.12 (2C), 140.13, 139.83 (2C), 134.36, 130.11, 129.08, 128.47, 127.44, 122.93 (2C), 122.44 (2C), 115.97 (2C), 109.41 (2C), 34.38 (2C), 31.92 (6C) ppm. HRMS (APCI) calculated for $C_{27}H_{28}NO_2$ $[M-H]^-$: 398.2120, found: 398.2123.

General Methodology for the Synthesis of Anhydrides 1−4. A mixture of acids **11**−**14** (1.00 g) and acetic anhydride (5 mL) was refluxed for 6 h (for acids **13** and **14**) or 4 h (for acids **11** and **12**). Then, the reaction mixture was concentrated in vacuo, and the residue was purified by column chromatography on silica gel using hexanes/dichloromethane (1:1) as the eluent. Compounds **1**, **2**, and **4** were further recrystallized from hexanes/chloroform (1:1), while compound **3** was recrystallized from a hexanes/toluene (1:1) mixture.

4-(9*H*-Carbazol-9-yl)benzoic anhydride (**1**) was obtained as a white solid in 35% yield (338 mg) from acid **11**. ^{1}H NMR (400 MHz, $CDCl_3$): δ = 8.46 (d, *J* = 8.4 Hz, 4H), 8.17 (d, *J* = 7.6 Hz, 4H), 7.83 (d, *J* = 8.4 Hz, 4H), 7.56 (d, *J* = 8.2 Hz, 4H), 7.47 (t, *J* = 7.7 Hz, 4H), 7.36 (t, *J* = 7.4 Hz, 4H) ppm. ^{13}C{H} NMR (101 MHz, $CDCl_3$): δ = 161.71 (2C), 143.87 (2C), 140.12 (4C), 132.59 (4C), 126.96 (2C), 126.77 (4C), 126.48 (4C), 124.18 (4C), 121.06 (4C), 120.69 (4C), 109.88 (4C) ppm. HRMS (APCI) calculated for $C_{38}H_{24}N_2O_3$ $[M]^+$: 556.1787, found: 556.1797. IR-spectrum (ATR): 3054.95, 1772.78, 1718.59, 1589.78, 1511.78, 1478.98, 1449.03, 1333.51, 1215.13, 1166.64, 1035.43, 1004.05, 831.48, 745.91, 720.24, 688.86, 415.03 cm^{-1}.

4-(3,6-Di-*tert*-butyl-9*H*-carbazol-9-yl)benzoic anhydride (**2**) was obtained as a white solid in 46% yield (448 mg) from acid **12**. ^{1}H NMR (400 MHz, $CDCl_3$): δ = 8.44 (d, *J* = 8.6 Hz, 4H), 8.17 (s, 4H), 7.82 (d, *J* = 8.6 Hz, 4H), 7.47−7.56 (m, 8H), 1.50 (s, 36H) ppm. ^{13}C{H} NMR (101 MHz, $CDCl_3$): δ = 161.89 (2C), 144.39 (2C), 144.16 (4C), 138.44 (4C), 132.56 (4C), 126.38 (2C), 126.17 (4C), 124.28 (4C), 124.14 (4C), 116.65 (4C), 109.45 (4C), 34.94 (4C), 32.10 (12C) ppm. HRMS (APCI) calculated for $C_{54}H_{56}N_2O_3$ $[M]^+$: 780.4291, found: 780.4289. IR-spectrum (ATR): 2955.11, 2865.26, 1777.06, 1720.01, 1603.06, 1513.21, 1471.85, 1363.46, 1216.56, 1165.21, 1043.99, 1004.05, 814.37, 610.42 cm^{-1}.

2-(9*H*-Carbazol-9-yl)benzoic anhydride (**3**) was obtained as a white solid in 64% yield (621 mg) from acid **13**. ^{1}H NMR (400 MHz, $CDCl_3$): δ = 7.95 (d, *J* = 7.6 Hz, 4H), 7.56 (ddd, *J* = 7.9, 7.0, 2.2 Hz, 2H), 7.30 (d, *J* = 7.6 Hz, 2H), 7.25 (td, *J* = 7.2, 1.2 Hz, 4H), 7.21−7.13 (m, 8H), 6.79 (d, *J* = 8.1 Hz, 4H) ppm. ^{13}C{H} NMR (101 MHz, $CDCl_3$): δ = 159.91 (2C), 141.38 (4C), 137.48 (2C), 134.66 (2C), 132.84 (2C), 130.34 (2C), 128.39 (2C), 127.73 (2C), 126.27 (4C), 123.58 (4C), 120.39 (4C), 120.19 (4C), 109.54 (4C) ppm. HRMS (ESI-TOF) calculated for $C_{38}H_{24}N_2O_3Na$ $[M + Na]^+$: 579.1685, found: 579.1686. IR-spectrum (ATR): 1788.47, 1724.29, 1597.36, 1497.52, 1450.46, 1314.97, 1230.82, 1203.72, 1015.46, 988.36, 785.84, 745.91, 723.09, 616.12, 419.31 cm^{-1}.

2-(3,6-Di-*tert*-butyl-9*H*-carbazol-9-yl)benzoic anhydride (**4**) was obtained as a white solid in 56% yield (545 mg) from acid **14**. ^{1}H NMR (400 MHz, $CDCl_3$): δ = 7.94 (d, *J* = 1.4 Hz, 4H), 7.53−7.49 (m, 2H), 7.23−7.31 (m, 6H), 7.15−7.17 (m, 4H), 6.73 (d, *J* = 8.6 Hz, 4H), 1.35 (s, 36H) ppm. ^{13}C{H} NMR (101 MHz, $CDCl_3$): δ = 160.26 (2C), 142.98 (4C), 139.86 (4C), 137.91 (2C), 134.28 (2C), 132.63 (2C), 129.83 (2C), 127.86 (2C), 127.78 (2C), 123.83 (4C), 123.63 (4C), 116.32 (4C), 109.02 (4C), 34.83 (4C), 32.17 (12C) ppm. HRMS (ESI-TOF) calculated for $C_{54}H_{56}N_2O_3Na$ $[M + Na]^+$: 803.4189, found: 803.4158. IR-spectrum (ATR): 2950.83, 2865.26, 1808.44, 1741.40, 1598.78, 1488.96, 1474.70, 1450.46, 1363.46, 1293.57, 1260.77, 1210.85, 1113.87, 996.92, 877.12, 807.24, 800.10, 773.01, 630.39 cm^{-1}.

■ ASSOCIATED CONTENT

Data Availability Statement

The data underlying this study are available in the published article and its Supporting Information.

Supporting Information

The Supporting Information is available free of charge at https://pubs.acs.org/doi/10.1021/acsami.6c11053.

Experimental procedures and characterization of the synthesized compounds; ORTEP diagrams for the X-ray structures and crystal data of compounds 1, 3, and 4; thermal and electrochemical data; (TD)DFT calculations data; additional photophysical spectra and data; NMR and IR spectra of the synthesized compounds (PDF)

Under mechanical stimulation, visible emission was indeed observed (MP4)

■ AUTHOR INFORMATION

Corresponding Authors

Juozas Vidas Grazulevicius – *Department of Polymer Chemistry and Technology, Kaunas University of Technology, Barsausko 59, Kaunas LT-51423, Lithuania;* orcid.org/0000-0002-4408-9727; Email: juozas.grazulevicius@ktu.lt

Mykhaylo A. Potopnyk – *Department of Organic Chemistry, Faculty of Chemistry, Ivan Franko National University of Lviv, Kyryla i Mefodiya 6, Lviv 79005, Ukraine; Institute of Organic Chemistry, Polish Academy of Sciences, Kasprzaka 44/52, Warsaw 01-224, Poland;* orcid.org/0000-0002-4543-2785; Email: potopnyk@gmail.com; mykhaylo.potopnyk@icho.edu.pl

Authors

Myroslava Aksionova – *Department of Organic Chemistry, Faculty of Chemistry, Ivan Franko National University of Lviv, Kyryla i Mefodiya 6, Lviv 79005, Ukraine*

Khrystyna Ivaniuk – *Department of Electronic Engineering, Lviv Polytechnic National University, Sviatoho Yura sq. 1, Lviv 79013, Ukraine; Institute of Organic Chemistry, Polish Academy of Sciences, Kasprzaka 44/52, Warsaw 01-224, Poland*

Roman Lytvyn – *Department of Organic Chemistry, Faculty of Chemistry, Ivan Franko National University of Lviv, Kyryla i Mefodiya 6, Lviv 79005, Ukraine; Institute of Organic Chemistry, Polish Academy of Sciences, Kasprzaka 44/52, Warsaw 01-224, Poland*; orcid.org/0000-0001-7086-9703

Stepan Kutsiy – *Department of Electronic Engineering, Lviv Polytechnic National University, Sviatoho Yura sq. 1, Lviv 79013, Ukraine; Institute of Organic Chemistry, Polish Academy of Sciences, Kasprzaka 44/52, Warsaw 01-224, Poland*; orcid.org/0000-0002-0757-6059

Oskar Kaszubowski – *Faculty of Chemistry, University of Wrocław, F. Joliot-Curie 14, Wrocław 50-383, Poland*

Vasyl Kinzhybalo – *Institute of Low Temperature and Structure Research, Polish Academy of Sciences, Okólna 2, Wrocław 50-422, Poland*; orcid.org/0000-0003-1060-0459

Asta Dabulienė – *Department of Polymer Chemistry and Technology, Kaunas University of Technology, Barsausko 59, Kaunas LT-51423, Lithuania*

Dmytro Volyniuk – *Department of Polymer Chemistry and Technology, Kaunas University of Technology, Barsausko 59, Kaunas LT-51423, Lithuania*; orcid.org/0000-0003-3526-2679

Mykola D. Obushak – *Department of Organic Chemistry, Faculty of Chemistry, Ivan Franko National University of Lviv, Kyryla i Mefodiya 6, Lviv 79005, Ukraine*; orcid.org/0000-0001-8146-9529

Complete contact information is available at: https://pubs.acs.org/doi/10.1021/acsami.6c11053

Author Contributions

Myroslava Aksionova and Roman Lytvyn: performed the synthesis. Khrystyna Ivaniuk: performed the electrochemical investigation. Roman Lytvyn: carried out the theoretical calculations. Asta Dabulienė: performed the thermal analysis. Oskar Kaszubowski and Vasyl Kinzhybalo: carried out chrystalographic analysis. Khrystyna Ivaniuk, Stepan Kutsiy, Dmytro Volyniuk, and Mykhaylo A. Potopnyk: performed the photophysical characterization. Khrystyna Ivaniuk and Dmytro Volyniuk: fabricated the OLEDs. Myroslava Aksionova, Roman Lytvyn, Khrystyna Ivaniuk, and Mykhaylo A. Potopnyk: wrote the original draft. Dmytro Volyniuk, Juozas V. Grazulevicius, and Mykhaylo A. Potopnyk: revised the draft. Mykhaylo A. Potopnyk, Mykola D. Obushak, and Juozas V. Grazulevicius: initiated, coordinated, and supervised the research and were responsible for funding acquisition. All authors contributed to discussions, reviewed and edited the manuscript, and approved the final version.

Notes

The authors declare no competing financial interest.

■ ACKNOWLEDGMENTS

The authors acknowledge the financial support of "Long-term program of support of the Ukrainian research teams at the Polish Academy of Sciences carried out in collaboration with the U.S. National Academy of Sciences with the financial support of external partners" (PAN.BFB.S.BWZ.330.022.2023). M.D.O. acknowledges financial support from the National Research Foundation of Ukraine (Project No. 2025.07/0221). M.A. gratefully acknowledges the Ministry of Education and Science of Ukraine for a scholarship. D.V. and A.D. thank the Research Council of Lithuania (project COLED, No S-MIP-24-2). The authors also sincerely thank Prof. Daniel T. Gryko and Prof. Agnieszka Szumna (Institute of Organic Chemistry PAS) for granting access to their research instruments.

■ DEDICATION

This manuscript is dedicated to the memory of Serhii Butenko (1999–2024), a PhD student and defender of Ukraine.

■ ABBREVIATIONS

TADF	thermally activated delayed fluorescence
RTP	room-temperature phosphorescence
OLED	organic light-emitting diode
IQE	internal quantum efficiency
D–A	donor–acceptor
SCXRD	single-crystal X-ray diffraction
NMR	nuclear magnetic resonance spectroscopy
IR	infrared spectroscopy
HRMS	high-resolution mass spectrometry
TGA	thermogravimetric analysis
DSC	differential scanning calorimetry
CV	cyclic voltammetry
IE	ionization energy
EA	electron affinity
TD-DFT	time-dependent density functional theory
HOMO	highest occupied molecular orbital
LUMO	lowest unoccupied molecular orbital
LE	locally excited
CT	charge-transfer
LEB	lowest-energy band
PLQYs	photoluminescence quantum yields
ISC/RISC	intersystem crossing/reverse intersystem crossing
TRPL	time-resolved photoluminescence
DF	delayed fluorescence
EL	electroluminescence
ITO	indium tin oxide
TPD	*N*,*N*′-bis(3-methylphenyl)-*N*,*N*′-diphenylbenzidine
mCP	1,3-bis(*N*-carbazolyl)benzene
EML	light-emitting layer
TSPO1	diphenyl[4-(triphenylsilyl)phenyl]phosphine oxide
TPBi	2,2′,2″-(1,3,5-benzenetriyl)tris(1-phenyl-1*H*-benzimidazole)
EQE	external quantum efficiency
CE	current efficiency
PE	power efficiency.

■ REFERENCES

(1) Dos Santos, J. M.; Hall, D.; Basumatary, B.; Bryden, M.; Chen, D.; Choudhary, P.; Comerford, T.; Crovini, E.; Danos, A.; De, J.; Diesing, S.; Fatahi, M.; Griffin, M.; Gupta, A. K.; Hafeez, H.; Hämmerling, L.; Hanover, E.; Haug, J.; Heil, T.; Karthik, D.; Kumar, S.; Lee, O.; Li, H.; Lucas, F.; Mackenzie, C. F. R.; Mariko, A.; Matulaitis, T.; Millward, F.; Olivier, Y.; Qi, Q.; Samuel, I. D. W.; Sharma, N.; Si, C.;

Spierling, L.; Sudhakar, P.; Sun, D.; Tankelevičiu¯tė, E.; Duarte Tonet, M.; Wang, J.; Wang, T.; Wu, S.; Xu, Y.; Zhang, L.; Zysman-Colman, E. The Golden Age of Thermally Activated Delayed Fluorescence Materials: Design and Exploitation. *Chem. Rev.* **2024**, *124* (24), 13736−14110.

(2) Zhou, Z.; Xie, X.; Sun, Z.; Wang, X.; An, Z.; Huang, W. Recent advances in metal-free phosphorescent materials for organic light-emitting diodes. *J. Mater. Chem. C* **2023**, *11* (9), 3143−3161.

(3) Palem, R. R.; Shimoga, G.; Lee, S.-H.; Kim, H.-S.; Bathula, C. Recent advances in OLED applications of TADF materials with decreased singlet-triplet energy gaps. *Coord. Chem. Rev.* **2026**, *556*, No. 217679.

(4) Wang, J.; Zhang, J.; Jiang, C.; Yao, C.; Xi, X. Effective Design Strategy for Aggregation-Induced Emission and Thermally Activated Delayed Fluorescence Emitters Achieving 18% External Quantum Efficiency Pure-Blue OLEDs with Extremely Low Roll-Off. *ACS Appl. Mater. Interfaces* **2021**, *13* (48), 57713−57724.

(5) Park, S.; Kwon, H.; Lee, H.; Lee, K.; Kang, S.; Kim, K. J.; Kim, T.; Park, J. Novel blue multiresonance thermally activated delayed fluorescence host materials, including Ge-based bulky groups. *J. Mater. Chem. C* **2024**, *12* (12), 4384−4391.

(6) Wang, J.; Niu, Y.; Jiang, Y.; Chen, Z.; Yao, C.; Yao, W.; He, M.; Zhang, J. Modulating the photophysical properties of isomeric thermally activated delayed fluorescence emitters through precise control of intra/intermolecular hydrogen bonding for nondoped OLEDs. *Mater. Today Chem.* **2025**, *47*, No. 102796.

(7) Ali, U.; Han, G.; Yi, Y. Switching the Luminescence between TADF and RTP for Organic D-A-D Emitters: The Role of D-A Connection Modes. *Adv. Theory Simul.* **2023**, *6* (2), No. 2200725.

(8) Li, P.; Lv, Q.; Sun, C.; Zhang, P.; Wang, X.; Yin, C.; Pan, Y.; Chen, R. Regulation of TADF and RTP Dual Emission via Internal and External Heavy-Atom Effects. *J. Phys. Chem. Lett.* **2024**, *15* (38), 9787−9794.

(9) Ferreira, M.; Decarli, N. O.; Nyga, A.; Erfurt, K.; Lingagouder, J.; de Sousa, L. E.; de Thieulloy, L.; de Silva, P.; Data, P. Multifunctional tris(triazolo)triazine-based emitter with dual-TADF, RTP, AIEE and AIDF properties. *J. Mater. Chem. C* **2024**, *12* (34), 13651−13664.

(10) Su, N.; Wang, J.; Yang, Y.; Yan, Z.; Zhou, L.; Zheng, Y.-X.; Ding, J. Chiral Single Molecule with Biphenyl Component Exhibiting Both TADF and RTP Emissions Enables Highly Efficient CP-OLEDs. *Angew. Chem., Int. Ed.* **2025**, *64* (40), No. e202512717.

(11) Kim, K.-H.; Kim, J.-J. Origin and Control of Orientation of Phosphorescent and TADF Dyes for High-Efficiency OLEDs. *Adv. Mater.* **2018**, *30* (42), No. 1705600.

(12) van der Zee, B.; Li, Y.; Wetzelaer, G.-J. A. H.; Blom, P. W. M. Triplet-Polaron-Annihilation-Induced Degradation of Organic Light-Emitting Diodes Based on Thermally Activated Delayed Fluorescence. *Phys. Rev. Applied* **2022**, *18*, No. 064002.

(13) Ko, S.-B.; Kang, S.; Kim, T. A Silane-Based Bipolar Host with High Triplet Energy for High Efficiency Deep-Blue Phosphorescent OLEDs with Improved Device Lifetime. *Chem. Eur. J.* **2020**, *26* (35), 7767−7773.

(14) Yang, G.-X.; Zhu, J.-J.; Tang, S.-S.; Tan, H.-J.; He, X.; Jian, J.-X.; Zheng, X.-H.; Tong, Q.-X. Effective Energy Transfer for Green, Orange, and Red Phosphorescent Organic Light-Emitting Diodes Based on a Bipolar Deep-Blue Emitter with Low Efficiency Roll-Off at High Brightness. *Adv. Photonics Res.* **2021**, *2* (7), No. 2100031.

(15) Muruganantham, S.; Jung, Y. H.; Kim, H. R.; Ham, J. H.; Braveenth, R.; Naveen, K. R.; Chae, M. Y.; Kwon, J. H. Unveiling a pyridine-based exciplex host for efficient stable blue phosphorescent organic light-emitting diodes. *J. Mater. Chem. C* **2025**, *13* (6), 2923−2931.

(16) Hosono, T.; Decarli, N. O.; Crocomo, P. Z.; Goya, T.; de Sousa, L. E.; Tohnai, N.; Minakata, S.; de Silva, P.; Data, P.; Takeda, Y. The regioisomeric effect on the excited-state fate leading to room-temperature phosphorescence or thermally activated delayed fluorescence in a dibenzophenazine-cored donor−acceptor−donor system. *J. Mater. Chem. C* **2022**, *10* (12), 4905−4913.

(17) Goto, S.; Nitta, Y.; Decarli, N. O.; de Sousa, L. E.; Stachelek, P.; Tohnai, N.; Minakata, S.; de Silva, P.; Data, P.; Takeda, Y. Revealing the internal heavy chalcogen atom effect on the photophysics of the dibenzo[a,j]-phenazine-cored donor−acceptor−donor triad. *J. Mater. Chem. C* **2021**, *9* (39), 13942−13953.

(18) Wex, B.; Kaafarani, B. R. Perspective on carbazole-based organic compounds as emitters and hosts in TADF applications. *J. Mater. Chem. C* **2017**, *5* (34), 8622−8653.

(19) Ledwon, P. Recent advances of donor-acceptor type carbazole-based molecules for light emitting applications. *Org. Electron.* **2019**, *75*, No. 105422.

(20) Kumar, A.; Oh, J.; Kim, J.; Jung, J.; Lee, M. H. Facile Color Tuning of Thermally Activated Delayed Fluorescence by Substituted Ortho-Carbazole-Appended Triarylboron Emitters. *Dyes Pigm.* **2019**, *168*, 273−280.

(21) Konidena, R. K.; Thomas, K. R. J.; Park, J. W. Recent Advances in the Design of Multi-Substituted Carbazoles for Optoelectronics: Synthesis and Structure-Property Outlook. *ChemPhotoChem* **2022**, *6* (10), No. e202200059.

(22) Wang, J.; Yang, Y.; Gu, F.; Zhai, X.; Yao, C.; Zhang, J.; Jiang, C.; Xi, X. Molecular engineering modulating the singlet−triplet energy splitting of indolocarbazole-based TADF emitters exhibiting AIE properties for nondoped blue OLEDs with EQE of nearly 20%. *ACS Appl. Mater. Interfaces* **2023**, *15* (51), 59643−59654.

(23) Zinchenko, H. M.; Ivaniuk, K.; Hotynchan, A.; Jean-Woldemar, E.; Marek-Urban, P. H.; Mech-Piskorz, J.; Ceborska, M.; Pander, P.; Kędra, K.; Chénais, S.; Angulo, G.; Durka, K.; Forget, S.; Potopnyk, M. A. Donor−Acceptor Benzochalcogenazolo-Based N,O-Coordinated Boron Difluoride Emitters Exhibiting Amplified Spontaneous Emission and Thermally Activated Delayed Fluorescence for Organic Light-Emitting Diodes. *ACS Appl. Mater. Interfaces* **2025**, *17* (52), 70722−70739.

(24) Takeda, Y.; Kaihara, T.; Okazaki, M.; Higginbotham, H.; Data, P.; Tohnai, N.; Minakata, S. Conformationally-flexible and moderately electron-donating units-installed D−A−D triad enabling multicolor-changing mechanochromic luminescence, TADF and room-temperature phosphorescence. *Chem. Commun.* **2018**, *54* (50), 6847−6850.

(25) Han, X.; Wang, X.; Wu, Y.; Zhao, J.; Liu, Y.; Shu, H.; Wu, X.; Tong, H.; Wang, L. Modulation of triplet-mediated emission from selenoxanthen-9-one-based D−A−D type emitters through tuning the twist angle to realize electroluminescence efficiency over 25%. *J. Mater. Chem. C* **2022**, *10* (19), 7437−7442.

(26) Hsiao, S.-H.; Lin, S.-W. Electrochemical synthesis of electrochromic polycarbazole films from *N*-phenyl-3,6-bis(*N*-carbazolyl)carbazoles. *Polym. Chem.* **2016**, *7* (1), 198−211.

(27) Zhang, F.; Liu, Q.; Chen, Y.; Zhai, L.; Liu, M.; Sun, J.; Mi, W.; Sun, M.; Lu, R. Mechanofluorochromism of D−π−A-Type Difluoroboron β-Carbonyl Cyclic Ketonate Complexes that Contain a Carbazole Unit. *Asian J. Org. Chem.* **2017**, *6* (11), 1659−1666.

(28) Okochi, K. D.; Monfregola, L.; Dickerson, S. M.; McCaffrey, R.; Domaille, D. W.; Yu, C.; Hafenstine, G. R.; Jin, Y.; Cha, J. N.; Kuchta, R. D.; Caruthers, M.; Zhang, W. Synthesis of Small-Molecule/DNA Hybrids through On-Bead Amide-Coupling Approach. *J. Org. Chem.* **2017**, *82* (20), 10803−10811.

(29) Wu, L.; Tiekink, M.; Giuliani, A.; Nahon, L.; Castellanos, S. Tuning photoionization mechanisms of molecular hybrid materials for EUV lithography applications. *J. Mater. Chem. C* **2019**, *7* (1), 33−37.

(30) Potopnyk, M. A.; Volyniuk, D.; Luboradzki, R.; Lazauskas, A.; Gražulevičius, J. V. Aggregation-Induced Emission-Active Carbazolyl-Modified Benzo[4,5]thiazolo[3,2-*c*]oxadiazaborinines as Mechanochromic Fluorescent Materials. *Eur. J. Org. Chem.* **2021**, *2021* (19), 2772−2781.

(31) Liu, W.; Liu, G.; Zhu, X.; Han, X.; Lu, A.; Lu, S.; Shi, L.; Hao, X.-Q.; Song, M.-P. Tailored metal−organic tetrahedral nanocages with aggregation-induced emission for an anticounterfeiting ink and stimulus-responsive luminescence. *New J. Chem.* **2022**, *46* (17), 8062−8068.

(32) Potopnyk, M. A.; Mech-Piskorz, J.; Angulo, G.; Ceborska, M.; Luboradzki, R.; Andresen, E.; Gajek, A.; Wisniewska, A.; Resch-

https://doi.org/10.1021/acsami.6c11053
ACS Appl. Mater. Interfaces XXXX, XXX, XXX−XXX

Genger, U. Aggregation/Crystallization-Induced Emission in Naphthyridine-Based Carbazolyl-Modified Donor-Acceptor Boron Dyes Tunable by Fluorine Atoms. *Chem. – Eur. J.* **2024**, *30* (22), No. e202400004.
(33) Ruchlin, C.; Castillo-Pazos, D. J.; Lasso, J. D.; Hamzehpoor, E.; Mikov, A.; Li, C.-J.; Perepichka, D. F. Divergent Synthesis and Crystal Engineering of Room-Temperature Phosphorescent Carbonyl-Bridged Triphenylamines. *Angew. Chem., Int. Ed.* **2025**, *64* (38), No. e202512446.
(34) Lee, Y. H.; Park, S.; Oh, J.; Shin, J. W.; Jung, J.; Yoo, S.; Lee, M. H. Rigidity-Induced Delayed Fluorescence by Ortho Donor-Appended Triarylboron Compounds: Record-High Efficiency in Pure Blue Fluorescent Organic Light-Emitting Diodes. *ACS Appl. Mater. Interfaces* **2017**, *9* (28), 24035−24042.
(35) Liu, R.; Liu, C.; Fu, C.; Zhu, Z.; Chen, K.; Li, C.; Wang, L.; Huang, Y.; Lu, Z. Ambient Phosphor with High Efficiency and Long Lifetime in Poly(Methyl Methacrylate) Through Charge-Transfer-Mediated Triplet Exciton Formation for Photolithography Applications. *Angew. Chem., Int. Ed.* **2024**, *63* (4), No. e202312534.
(36) Kim, J.; Lee, T.; Ryu, J. Y.; Lee, Y. H.; Lee, J.; Jung, J.; Lee, M. H. Highly Emissive ortho-Donor−Acceptor Triarylboranes: Impact of Boryl Acceptors on Luminescence Properties. *Organometallics* **2020**, *39* (12), 2235−2244.
(37) Mubarok, H.; Lee, W.; Lee, T.; Kim, D.; Jung, J.; Lee, M. H. Impact of Boron Acceptors on the TADF Properties of Ortho-Donor-Appended Triarylboron Emitters. *Front. Chem.* **2020**, *8*, No. 538.
(38) Narita, H.; Min, H.; Kubo, N.; Hattori, I.; Yasuda, T.; Yamaguchi, S. Bis-Ortho-Donor-Modification of Boracyclic π-Electron Systems beyond Steric Protection to Produce Thermally Activated Delayed Fluorescence Materials. *Angew. Chem., Int. Ed.* **2024**, *63* (30), No. e202405412.
(39) Zhang, T.; Xiao, Y.; Wang, H.; Kong, S.; Huang, R.; Ka-Man Au, V.; Yu, T.; Huang, W. Highly Twisted Thermally Activated Delayed Fluorescence (TADF) Molecules and Their Applications in Organic Light-Emitting Diodes (OLEDs). *Angew. Chem., Int. Ed.* **2023**, *62* (39), No. e202301896.
(40) Zhou, Y.; Qu, L.; Yi, S.; Wang, C.; Chen, X.; Tang, S.; Tang, H.; Li, Y.; Wang, K.; Zhao, Y.; Yang, C. Dual Promotion of Phosphorus Groups for Ultralong Room Temperature Phosphorescence with High Efficiency. *Adv. Opt. Mater.* **2023**, *11* (3), No. 2201904.
(41) Potopnyk, M. A.; Kravets, M.; Luboradzki, R.; Volyniuk, D.; Sashuk, V.; Grazulevicius, J. V. Carbazole-modified thiazolo[3,2-c][1,3,5,2]oxadiazaborinines exhibiting aggregation-induced emission and mechanofluorochromism. *Org. Biomol. Chem.* **2021**, *19* (2), 406−415.
(42) Kutsiy, S.; Volyniuk, D.; Sahoo, S. R.; Ceborska, M.; Wisniewska, A.; Stakhira, P.; Grazulevicius, J. V.; Baryshnikov, G. V.; Potopnyk, M. A. Sterically Tuned Ortho-Phenylene-Linked Donor−Acceptor Benzothiazole-Based Boron Difluoride Complexes as Thermally-Activated Delayed Fluorescence Emitters for Organic Light-Emitting Diodes. *ACS Appl. Mater. Interfaces* **2024**, *16* (44), 60633−60647.
(43) Clevers, S.; Coquerel, G. Kryptoracemic compound hunting and frequency in the Cambridge Structural Database. *CrystEngComm* **2020**, *22 (43)*, 7407−7419.
(44) Yang, S.; Wu, D.; Gong, W.; Huang, Q.; Zhen, H.; Ling, Q.; Lin, Z. Highly efficient room-temperature phosphorescence and afterglow luminescence from common organic fluorophores in 2D hybrid perovskites. *Chem. Sci.* **2018**, *9* (48), 8975−8981.
(45) Gottlieb, H. E.; Kotlyar, V.; Nudelman, A. NMR Chemical Shifts of Common Laboratory Solvents as Trace Impurities. *J. Org. Chem.* **1997**, *62* (21), 7512−7515.
(46) Rigaku. *CrysAlisPro (ver. 1.171.44.122a)*; Rigaku Oxford Diffraction, **2025**.
(47) Sheldrick, G. M. SHELXT - Integrated space-group and crystal structure determination. *Acta Crystallogr.* **2015**, *71*, 3−8.
(48) Sheldrick, G. M. Crystal Structure Refinement with SHELXL. *Acta Crystallogr.* **2015**, *71*, 3−8.
(49) Dolomanov, O. V.; Bourhis, L. J.; Gildea, R. J.; Howard, J. A. K.; Puschmann, H. OLEX2: a complete structure solution, refinement and analysis program. *J. Appl. Cryst.* **2009**, *42*, 339−341.
(50) Hladka, I.; Lytvyn, R.; Volyniuk, D.; Gudeika, D.; Grazulevicius, J. V. W-shaped bipolar derivatives of carbazole and oxadiazole with high triplet energies for electroluminescent devices Author links open overlay panel. *Dyes Pigm.* **2018**, *149*, 812−821.

https://doi.org/10.1021/acsami.6c11053
ACS Appl. Mater. Interfaces XXXX, XXX, XXX−XXX